Geophysical and Astrophysical Fluid Dynamics
Vol. 98, No. 2, April 2004, pp. 153–169

Taylor & Francis
Taylor & Francis Group

VARYING THE SPHERICAL SHELL GEOMETRY IN ROTATING THERMAL CONVECTION

F.M. AL-SHAMALI[a,*], M.H. HEIMPEL[a] and J.M. AURNOU[b,*]

[a]*Department of Physics, University of Alberta, Edmonton, T6G 2J1, Canada;*
[b]*Department of Terrestrial Magnetism, Carnegie Institution of Washington, Washington, DC, USA*

(Received 20 February 2003; In final form 30 October 2003)

The effect of spherical shell geometry on rapidly-rotating thermal convection is studied in a suite of high resolution three-dimensional numerical simulations. The geometry is characterized by the radius ratio, $\chi = r_i/r_o$, where r_i is the inner shell radius, and r_o is the outer shell radius. In this study, χ is varied over the broad range 0.10 to 0.92 in calculations of Boussinesq rotating convection subject to isothermal, rigid boundary conditions. Simulations are performed at Prandtl number $Pr = 1$ and for Ekman numbers $E = 10^{-3}$, 3×10^{-4} and 10^{-4}. Near the onset of convection, the flow takes the form of rolls aligned parallel to the rotation axis and situated adjacent to the inner shell equator. The dimensionless azimuthal wavelength, λ_c, of the rolls is found to be independent of the shell geometry, only varying with the Ekman number. The critical wave number, m_c, of the columnar rolls increases in direct proportion to the inner boundary circumference. For our simulations the critical Rayleigh number Ra_c at which convection first occurs varies in proportion to $E^{-1.16}$; a result that is consistent with previous work on rotating convection. Furthermore, we find that Ra_c is a complex function of χ. We obtain the relation $Ra_c\, E^{1.16} = 0.21/\chi^2 + 22.4\sqrt{(1-\chi)(1+\chi)}$, which adequately fits all our results. In supercritical convection calculations the flows form quasi-geostrophic sheet-like structures that are elongated in the radial direction, stretching from the inner boundary toward the outer boundary.

Keywords: Thermal convection; Rotation; Shell geometry; Radius ratio

1 INTRODUCTION

Understanding thermal convection in a rapidly rotating spherical shell is of great importance in studying the dynamo processes that occur in planetary cores. In particular, how convection is affected by planetary core spherical shell geometry, which can vary due to planetary size, composition and cooling history, has not been well quantified. Self-sustained planetary dynamos appear to be driven by fluid motions in their electrically conducting cores. Indeed, it is likely that the planets and planetary satellites with large observed intrinsic magnetic fields have vigorously convecting cores with $Ra \gg Ra_c$, where Ra is the Rayleigh number and Ra_c is the critical Rayleigh number for the onset of convection. Although it may appear that the applicability of studying

*Corresponding author. Present address: Department of Earth and Space Sciences, University of California, Los Angeles, 90095-1567, USA. E-mail: aurnou@ucla.edu

ISSN 0309-1929 print: ISSN 1029-0419 online
DOI: 10.1080/03091920410001659281

the onset of rotating (nonmagnetic) convection is limited, it is, in practice, crucial to establish how the conditions that govern the onset of convection vary for different planetary core geometries. Thus a purpose of this study is to obtain critical Rayleigh numbers for a broad range of spherical shell geometries, and to provide a baseline by which to scale rotating convection and dynamo models with more vigorous convection.

A great deal of previous work has focused on understanding rotating convection relevant to flows in planetary cores and in the solar convection zone. Recent theoretical studies include those of Yano (1992), Zhang and Jones (1993), and Jones *et al.* (2000). Numerical work includes studies by Zhang (1992), Glatzmaier and Olson (1993), Dormy (1997), Tilgner and Busse (1997), Christensen *et al.* (1999), and Miesch *et al.* (2000). Experimental studies include Busse and Carrigan (1975), Cardin and Olson (1992, 1994), Sumita and Olson (2000) and Aubert *et al.* (2001). The general pattern of convection in all these studies takes the form of columnar convection rolls that are aligned parallel to the axis of rotation. The columnar structure of the rolls results because strong Coriolis forces act to rigidify the fluid parallel to the rotation axis (Proudman, 1916). Thus, in the high rotation rate regime, rotation stabilizes the fluid such that the critical Rayleigh number tends to vary with the Ekman number E as $Ra_c \propto E^{-4/3}$ (Chandrasekhar, 1961; Roberts, 1968).

The geometry of the Earth's core ($\chi = 0.35$) and that of the solar convection zone ($\chi = 0.7$) have been the focus of the vast majority of previous studies. Exceptions include Jones *et al.* (2000), the strongly-truncated, two and a half dimensional models of rotating convection and dynamo action by Drew (1991) and Morrison and Fearn (2000), as well as the kinematic dynamo study of Schubert and Zhang (2001). Additionally, Sakuraba and Kono (1999) and Roberts and Glatzmaier (2001) modeled convection driven dynamo action in fully three-dimensional models with differing inner core sizes.

Here we present a systematic study of rotating convection between spherical shells for a broad range of radius ratio values. Results are obtained from high resolution, fully three-dimensional and weakly truncated numerical models. In Section 2 we discuss the relevant equations of motions and the numerical techniques employed in their solution; the results of the numerical simulations are presented in Section 3; further discussion of the results and comparisons with previous work are presented Section 4; in Section 5 we summarize our findings. In a following paper, we will discuss how spherical shell geometry affects dynamo action.

2 METHOD

2.1 Governing Equations

In this study, we perform a series of three-dimensional numerical simulations of thermal convection in rotating spherical shells. The governing equations are

$$E\left(\frac{\partial \mathbf{u}}{\partial t} + \mathbf{u}\cdot\nabla\mathbf{u} - \nabla^2\mathbf{u}\right) + 2\,\hat{\boldsymbol{z}}\times\mathbf{u} + \nabla P = \left(\frac{ERa}{Pr}\right)\frac{g}{g_o}\,T\hat{\boldsymbol{r}}, \tag{1}$$

$$\frac{\partial T}{\partial t} + \mathbf{u}\cdot\nabla T = \left(\frac{1}{Pr}\right)\nabla^2 T, \tag{2}$$

$$\nabla\cdot\mathbf{u} = 0, \tag{3}$$

which are solved simultaneously to determine the fluid velocity vector **u** and the temperature field T.

The calculations are performed subject to a constant temperature difference, ΔT, that is maintained between isothermal, mechanically rigid, inner and outer boundaries, r_i and r_o, respectively. The boundaries of the shell co-rotate with angular velocity $\Omega\hat{z}$. Convection is driven by central gravity $g(r)$ which increases linearly with radius and has a value g_o at the outer surface.The fluid is Boussinesq and its physical properties are characterized by α, the thermal expansion coefficient, ν, the kinematic viscosity, and κ, the thermal diffusivity.

2.2 Nondimensional Parameters

Equations (1)–(3) have been nondimensionalized using the spherical shell thickness $D = r_o - r_i$ for length, D^2/ν for time, ν/D for velocity, $\rho\nu\Omega$ for pressure and ΔT for temperature. The controlling nondimensional parameters for this system are the following: the Rayleigh number

$$Ra = \frac{\alpha g_o \Delta T D^3}{\kappa\nu}, \tag{4}$$

which is the ratio of buoyancy to viscous forces; the Ekman number

$$E = \frac{\nu}{\Omega D^2}, \tag{5}$$

which is the ratio of the viscous to Coriolis forces; and the Prandtl number

$$Pr = \frac{\nu}{\kappa}, \tag{6}$$

which is the ratio of the viscous and the thermal diffusivities of the working fluid. In the calculations presented here, the Prandtl number is held fixed at $Pr = 1$.

The radius ratio

$$\chi = \frac{r_i}{r_o}, \tag{7}$$

which is the focus of this study, defines the geometry of the spherical shell. In planetary cores, the radius ratio describes the size of the solid inner core relative to the fluid outer core. Thus, the nondimensionalized values of r_i and r_o are given by the relations

$$r_i = \frac{\chi}{1-\chi} \quad \text{and} \quad r_o = \frac{1}{1-\chi}. \tag{8}$$

In our calculations, we studied the effects of varying the radius ratio χ, on the onset of convection, at three different Ekman numbers ($E = 10^{-3}$, 3×10^{-4} and 10^{-4}).

Note that for a fixed value of D, the radii of the inner and outer shells both increase with χ (see Table I). Alternatively, r_o may be held constant so that the shell thickness D

TABLE I Spherical shell dimensions for various values of χ

χ	r_i	r_o	D
0.15	0.176	1.176	1
0.35	0.538	1.538	1
0.55	1.222	2.222	1
0.75	3.000	4.000	1

decreases as r_i and χ increase. This parameterization applies directly to a planet with a growing inner core. In this case, the Ekman number would increase as a function of decreasing shell thickness D for constant fluid viscosity ν and planetary rotation rate Ω. However, the limitations of present-day computational resources force us to use rather large E values. Thus, we argue that further increasing the Ekman number with increasing χ does not provide a good analogue to a planetary core, where E remains small even at very high χ values. Consider that in the Earth's core the Ekman number is estimated to be of order $E \sim 10^{-15}$, using $D = 2260\,\text{km}$ (i.e., $\chi = 0.35$), $\Omega = 7.27 \times 10^{-5}\,\text{s}^{-1}$ and $\nu \sim 10^{-6}\,\text{m}^2/\text{s}$. If the thickness of the Earth's fluid outer core were to decrease to $D = 100\,\text{km}$ (i.e., $\chi = 0.97$), the Ekman number would increase to a value of $E \sim 5 \times 10^{-14}$. Although E has increased by a factor of ~ 500, the rotational forces in the fluid are still dominant relative to viscous forces. Therefore, little qualitative change in the flow regime should result. In contrast, were we to do this in our simulations, the Ekman number would increase, from 3×10^{-4} up to 1.5×10^{-1}. For such a large final value of E, the fluid dynamics are no longer dominated by rotational forces and the results are not relevant to planetary core flows. So that this does not occur in our present calculations, we choose to define the Ekman number as $E = \nu/\Omega D^2$ based on a fixed shell thickness $D = 1$, while changing the value of χ.

2.3 Description of the Model and Calculations

The spherical dynamo code used here was originally developed by Glatzmaier and has been modified by Christensen and Wicht. We are presently running Wicht's version MAGIC 2.0 (Wicht, 2002). The numerical technique is described in Glatzmaier and Olson (1993) and Olson and Glatzmaier (1995) and uses the spectral transform method to solve Eqs. (1)–(3) simultaneously. The fields are expanded in the radial direction using Chebyshev polynomials and in the latitudinal and longitudinal directions using spherical harmonics. No hyperdiffusivities are used in any of our calculations.

In this study, we perform calculations at three different values of the Ekman number. The largest group of calculations are performed at $E = 3 \times 10^{-4}$. Smaller groups of calculations are performed at $E = 10^{-3}$ and 10^{-4}. Several sets of calculations are made using differing numerical grids in the radial r, latitudinal θ and azimuthal ϕ directions. We impose longitudinal symmetry in many of the calculations. Periodic conditions are employed on the bounding meridional planes of the truncated numerical domains used in these cases. For example, calculations with 4-fold longitudinal symmetry require 1/4 the number of points in the ϕ-direction and tend to run roughly 4 times faster than the full sphere calculations. Most of the runs are initialized to zero velocity

TABLE II Parameters for the calculations in this study. Column 1: radius ratio; Columns 2, 3 and 4: numbers of grid points in the radial r, longitudinal ϕ and latitudinal θ directions, respectively; Column 5: imposed longitudinal symmetry; Column 6: maximum spherical harmonic degree and order; Column 7: initial temperature perturbation to the conductive state

χ	*r-Levels*	*ϕ-Levels*	*θ-Levels*	*ϕ-Symmetry*	l_{max}	*Initial temp.*
$E = 10^{-3}$						
(0.10)	41	160	80	Full sphere	53	Random
(0.15 and 0.35)	33	128	64	Full sphere	42	Random
(0.55)	33	160	80	Full sphere	53	Random
(0.75)	41	256	128	Full sphere	85	Random
(0.85 and 0.90)	49	640	320	8-fold	213	Random
$E = 3 \times 10^{-4}$						
(0.10–0.35)	49	256	128	Full sphere	85	Random
(0.15–0.60)	49	320	160	4-fold	106	Random
(0.65–0.90)	49	576	288	4-fold	192	l, $m = 4$
(0.35)	49	640	320	8-fold	213	Random
(0.80, 0.90 and 0.92)	49	960	480	8-fold	320	Random
$E = 10^{-4}$						
(0.15 and 0.25)	49	192	96	Full sphere	64	Random
(0.35)	49	256	128	Full sphere	85	Random
(0.55)	49	480	240	4-fold	160	Random
(0.65, 0.75 and 0.80)	49	576	288	4-fold	192	Random

field and a radial conductive temperature gradient ($l = 0$, $m = 0$) with random thermal noise imposed as a perturbation. Time-stepping in these calculations continues until the convection has reached steady state. In thin shells, larger grids with maximum spherical harmonic degree $l_{\max}$ up to 192 are found to be necessary in order to resolve the high wave number flow features that are produced in such high χ shells. The detailed attributes of the calculations are given in Table II.

3 RESULTS

3.1 Critical Rayleigh Number

The onset of convection occurs at the critical Rayleigh number, Ra_c. For $Ra < Ra_c$, any initial perturbations decay and the heat transfer is maintained through conduction only. For $Ra > Ra_c$, convective motions can be sustained and the fluid's kinetic energy tends to grow monotonically as a function of $(Ra - Ra_c)$. For asymptotically small E the linear stability theory predicts that the critical Rayleigh number Ra_c will vary in proportion to $E^{-\gamma}$, where $\gamma = 4/3$; for larger E, outside the asymptotic regime, γ can take on values between 0 and 4/3 (Chandrasekhar, 1961).

Figure 1 shows the steady-state kinetic energy density plotted as a function of Ra. Here the kinetic energy density is defined as the total kinetic energy divided by the spherical shell volume. The tag on each line shows the corresponding radius ratio value. Note that for Ra close to Ra_c, the kinetic energy density varies linearly with the Rayleigh number. This allows us to make precise extrapolations to the critical Rayleigh number.

In Fig. 2 we present estimates of Ra_c determined by extrapolating the results shown in Fig. 1 to zero kinetic energy density. These Ra_c estimates are also presented

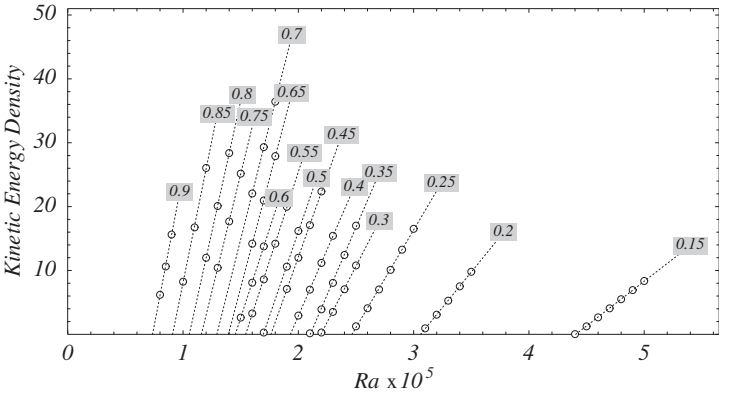

FIGURE 1 The fluid kinetic energy density, as a function of the Rayleigh number, calculated in spherical shells with different geometries. The graph corresponds to the $E = 3 \times 10^{-4}$ calculations performed using 4-fold ϕ-symmetry. The tag on each line showsthe corresponding radius ratio.

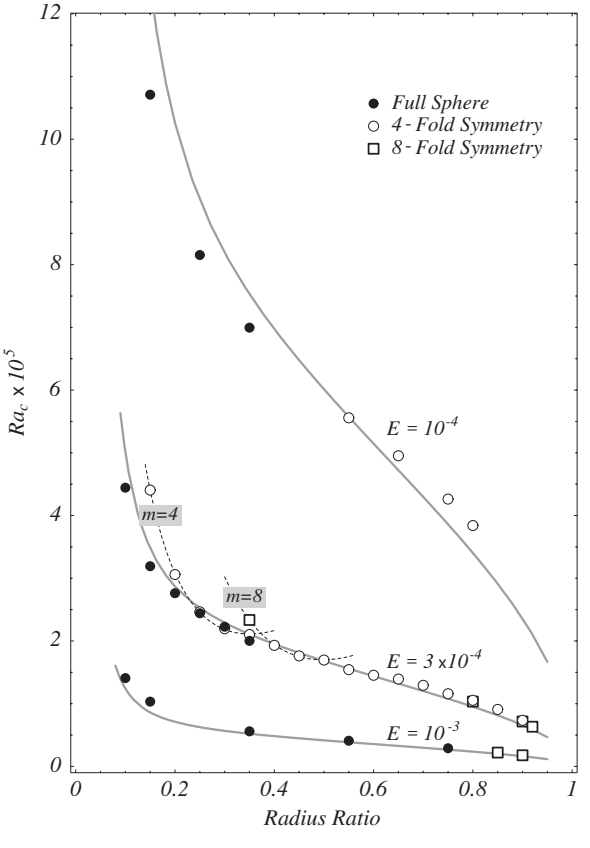

FIGURE 2 The critical Rayleigh number Ra_c, for the onset of convection in a rotating spherical shell, as a function of the radius ratio χ at $Pr = 1$ using three different Ekman numbers. Filled circles represent fully spherical calculations, open circles represent calculations with imposed 4-fold longitudinal symmetry and squares represent calculations with imposed 8-fold longitudinal symmetry. The three solid grey curves are produced using Eqs. (9) and (10) for the three different Ekman numbers. The dashed lines connect $E = 3 \times 10^{-4}$ cases where convection onsets as an $m = 4$ or as an $m = 8$ instability.

TABLE III Critical Rayleigh numbers and wavenumbers determined for the $E = 3 \times 10^{-4}$ calculations using full sphere, 4-fold and 8-fold symmetries

Radius ratio χ	*Full sphere*		*4-Fold symmetry*		*8-Fold symmetry*	
	$Ra_c \times 10^5$	m_c	$Ra_c \times 10^5$	m_c	$Ra_c \times 10^5$	m_c
0.10	4.44	1				
0.15	3.19	2	4.40	4		
0.20	2.76	3	3.06	4		
0.25	2.44	3	2.46	4		
0.30	2.23	4	2.20	4		
0.35	2.00	5	2.10	4	2.34	8
0.40			1.93	8		
0.45			1.76	8		
0.50			1.70	8		
0.55			1.54	12		
0.60			1.45	16		
0.65			1.39	16		
0.70			1.29	20		
0.75			1.16	28		
0.80			1.05	36	1.03	40
0.85			0.91	52		
0.90			0.74	92	0.72	88
0.92					0.63	104

TABLE IV Critical Rayleigh numbers and wave numbers determined for the $E = 10^{-3}$ and $E = 10^{-4}$ calculations

Radius ratio	$E = 10^{-3}$		$E = 10^{-4}$	
χ	$Ra_c \times 10^5$	m_c	$Ra_c \times 10^5$	m_c
0.10	1.41			
0.15	1.03	2	10.71	3
0.25			8.15	5
0.35	0.56	4	7.00	7
0.55	0.41	9	5.56	16
0.65			4.95	24
0.75	0.29	20	4.26	40
0.80			3.84	56
0.85	0.22	40		
0.90	0.18	64		

in Tables III and IV. The filled circles in Fig. 2 represent values obtained from full sphere calculations without any imposed symmetry. Open circles and squares represent values obtained from calculations with 4-fold and 8-fold imposed longitudinal symmetries, respectively. Two dashed lines are also shown in Fig. 2. The dashed line with the $m = 4$ tag connects all the $E = 3 \times 10^{-4}$ cases where convection onsets as an $m = 4$ instability (irrespective of imposed symmetry). The dashed line with the $m = 8$ tag connects the $E = 3 \times 10^{-4}$ cases that onset as an $m = 8$ instability.

The Ra_c values corresponding to the three Ekman numbers in Fig. 2 form three separate groups that vary similary with χ. This indicates that the dependence of Ra_c on E and χ is separable, and may be described by an equation of the form $Ra_c E^\gamma = f(\chi)$, where the value of γ and the function $f(\chi)$ must be determined. Thus, we fit all our Ra_c results (excepting the first two points in the 4-fold symmetry column in Table III and the first point in the 8-fold symmetry column in Table III)

with the following relationship

$$Ra_c E^{\gamma} = \frac{C_1}{\chi^2} + C_2 \left(\frac{1-\chi}{1+\chi} \right)^{1/2}, \tag{9}$$

where

$$\gamma = 1.16, \quad C_1 = 0.21\ , \quad \text{and } C_2 = 22.4 \tag{10}$$

are obtained from the fitting process.

Figure 3 shows our results plotted in terms of a modified critical Rayleigh number $Ra_c E^{\gamma}$, where $\gamma = 1.16$, as determined by the fit to (9). With this rescaling of the y-axis, our results collapse from three distinct curves in Fig. 2 onto one curve in Fig. 3. The solid grey curve is produced using (9) and (10).

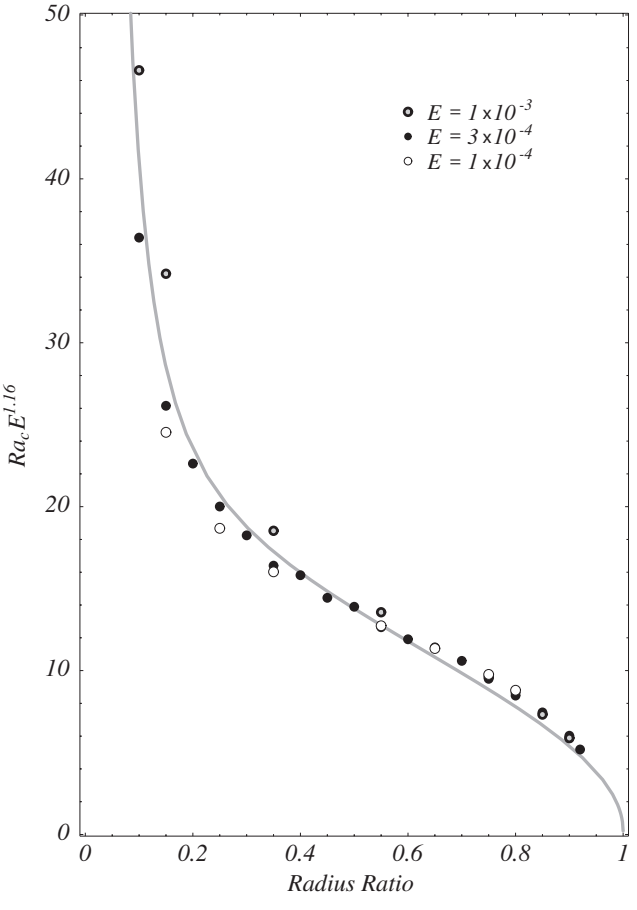

FIGURE 3 Modified critical Rayleigh number $Ra_c E^{1.16}$ plotted as a function of radius ratio χ. Points plotted are the same as in Fig. 2. Here, shaded circles, filled circles, and open circles represent results from numerical calculations with Ekman numbers $E = 10^{-3}$, 3×10^{-4} and 10^{-4}, respectively. The solid grey curve is produced using (9).

The right-hand side of (9) describes the χ variation of Ra_c. The first term models the Ra_c results in the low χ, thick shell regime while the second term models the Ra_c results in the high χ, thin shell regime.

In the thick shell regime, $Ra_c E^\gamma$ varies approximately as $1/\chi^2$. We argue that this behavior is due to the product of two effects. First, gravity varies linearly with radius in our simulations. Therefore, gravity at the inner shell boundary is proportional to χ. Convection columns first form just outside the tangent cylinder (defined as the imaginary cylinder that is aligned with the rotation axis and circumscribes the inner core equator). Although the gravitational acceleration at the inner shell, g_i, decreases with decreasing χ value, the Rayleigh number Ra, which is defined in terms of g_o, does not account for this effect. It follows that Ra_c must vary as $1/\chi$ in response to the dependence of g_i on χ. Second, the studies of Busse (1970) and Tilgner and Busse (1997) found that varying spherical boundary curvature also leads to a factor of $1/\chi$ variation in Ra_c. Thus, the first term in (9) is obtained as a product of two $1/\chi$ contributions, scaled by C_1.

In the thin shell regime described by $\chi \gtrsim 0.70$, $Ra_c E^\gamma$ varies roughly as $\sqrt{(1-\chi)/(1+\chi)}$. This relation has been adapted from the results of the study of Zhang and Greed (1998). They found that, for a rapidly rotating cylinder with flat, mechanically rigid ends and cylindrically radial gravity, the critical Rayleigh number varies as the inverse of the cylinder aspect ratio H/D, where H is cylinder height and D is the shell width. Thus, convection occurs most easily in cases with large aspect ratio, such that the fluid volume in the Ekman boundary layers is small compared to the total fluid volume. In our spherical shell results, we treat H as the height along the tangent cylinder, $2\sqrt{r_o^2 - r_i^2}$. This term adequately predicts the decrease in Ra_c for $\chi \gtrsim 0.70$ where H/D becomes increasingly large (see Fig. 2). No contribution from spherical shell curvature is required to explain our Ra_C results in this regime. This agrees with the previous findings of Zhang (1992) where it is argued that curvature effects are second order in E in the vicinity of the equator.

3.2 Flow Patterns

Figure 4 shows instantaneous patterns of the temperature field and the radial velocity field from calculations close to the onset of convection at $Ra = 1.1Ra_c$ and $E = 3 \times 10^{-4}$. The rows, from top to bottom, show results from cases at $\chi = 0.25$, 0.50 and 0.75, respectively. The left and middle columns show, respectively, color images of the temperature and radial velocity fields in the equatorial plane. The right-hand column shows radial velocity isosurfaces in the shell and color images in the equatorial plane. Blue colors represent low or negative values and red indicate high or positive values.

Near the onset of convection, the convecting fluid forms ordered convection rolls parallel to the rotation axis. The rolls are produced in pairs with opposite vorticity, transporting hot fluids from the inner toward the outer shell surfaces and vice versa. The columns in Fig. 4 tilt slightly in the prograde direction and extend from the edge of the tangent cylinder to roughly mid-shell, $(r_i + D/2)$, for all three χ values shown. The columns form adjacent to the tangent cylinder in all our calculations because the temperature gradient is steepest adjacent to the inner shell boundary. The fluid is convectively stable for $r > (r_i + D/2)$ irrespective of the value of χ. This occurs because

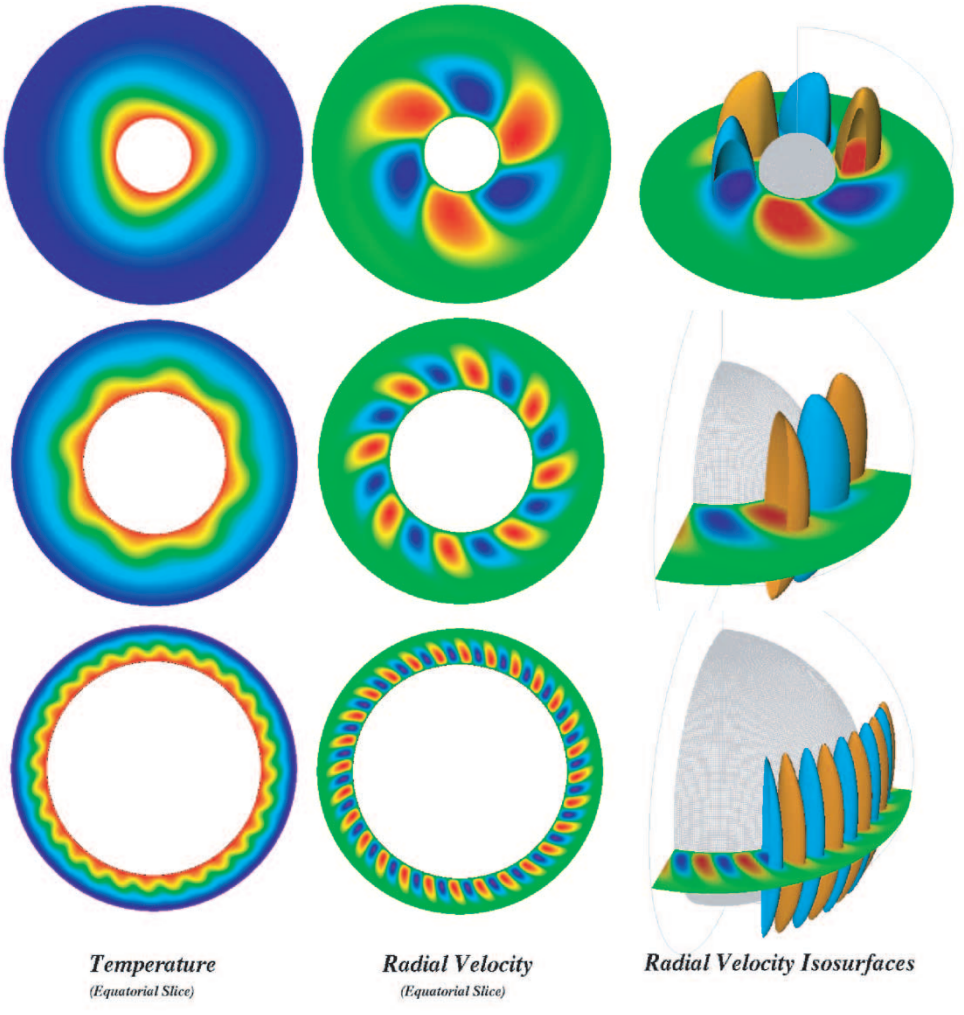

FIGURE 4 Temperature and radial velocity, calculated at $Ra = 1.1Ra_c$ and $E = 3 \times 10^{-4}$ for spherical shells with different geometries: $\chi = 0.25$ in the first row, $\chi = 0.50$ in the second row and $\chi = 0.75$ in the third row. The first and second columns show temperature and radial velocity fields, respectively, in the equatorial plane. The third column shows radial velocity isosurfaces as well as radial velocity contours in the equatorial plane. The color scheme ranges from red for high or positive values to blue for low or negative values.

the temperature gradient decreases as $1/r^2$ away from its maximum value at r_i (see Kono and Roberts, 2001).

3.3 Critical Wavenumber

The critical azimuthal wavenumber, m_c, represents the number of azimuthally-periodic columnar flow structures that form at the onset of convection. Figure 5 and Tables III and IV contain the values of m_c obtained in our calculations for different spherical shell

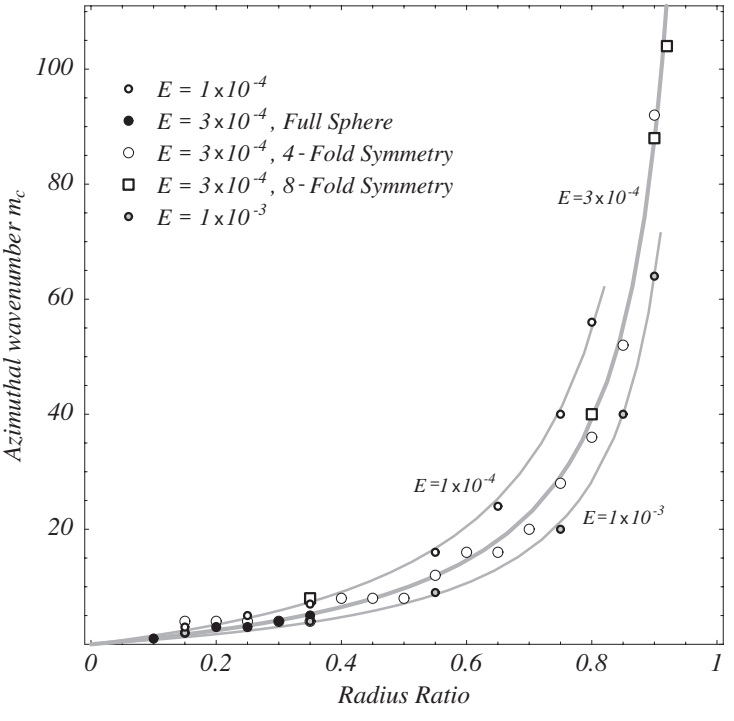

FIGURE 5 The critical azimuthal wavenumber, m_c, as a function of χ. The three continuous curves represent the best fits to (11).

TABLE V Dimensionless azimuthal wavelengths, λ_c, obtained from the best fits (second column) to the azimuthal wavenumbers. The third column contains the values of λ_c for convection columns in a rapidly rotating sphere, as predicted by Busse (1970)

E	*Azimuthal wavelength* λ_c	
	Best fit	*Busse (1970)*
10^{-3}	0.89	0.86
3×10^{-4}	0.65	0.57
10^{-4}	0.46	0.40

radius ratios. These are fit by the relationship

$$m_c = \frac{1}{\lambda_c}\frac{2\pi r_i}{D} = \frac{2\pi}{\lambda_c}\left(\frac{\chi}{1-\chi}\right), \tag{11}$$

where λ_c is defined here as the dimensionless azimuthal wavelength of instability along the inner shell boundary. The values of λ_c that produce the best fits to our results are presented in Table V. In Fig. 5, these fits are shown as the three solid grey curves.

Equation (11) can be understood on the basis of a simple geometrical relationship. For fixed values of E, the critical column length-scale, $\lambda_c D$, is constant. However,

the inner shell circumference $2\pi r_i$ increases with χ. Thus, the critical wavenumber increases in proportion to the circumference of the inner shell boundary.

3.4 Supercritical Convection

Figure 6 shows instantaneous patterns of the temperature field and the radial velocity field from calculations at $Ra = 5.0Ra_c$, $E = 3 \times 10^{-4}$ and $\chi = 0.25$, 0.50 and 0.75. The planform of convection is no longer purely periodic. Convection now fills the entire region outside the tangent cylinder, whereas the region inside the tangent cylinder is still subcritical to convective motions. For all three radius ratios, the convective motions occur along quasi-geostrophic sheets that extend nearly radially outward from r_i to r_o. This demonstrates that meridional motions are dominant relative to zonal motions. The convective wavenumbers along the inner boundary are $m \simeq 20 \sim 7m_c$ at $\chi = 0.25$; $m \simeq 32 \sim 4m_c$ at $\chi = 0.50$ and $m \simeq 80 \sim 3m_c$ at $\chi = 0.75$.

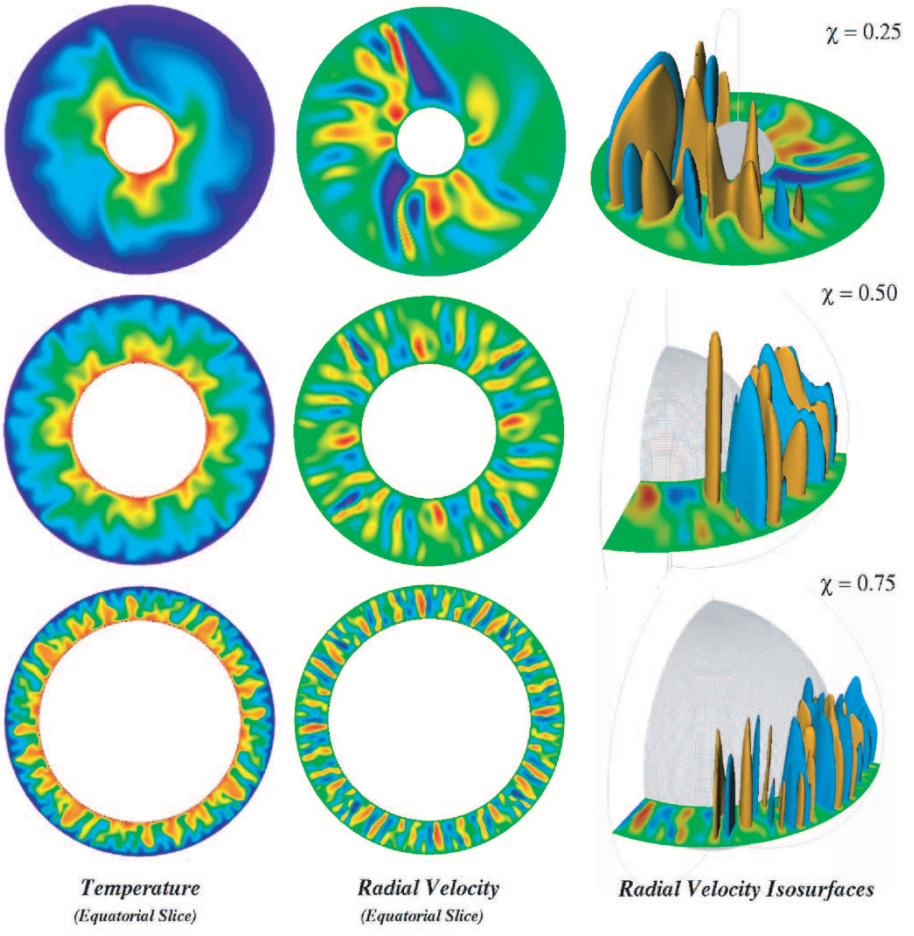

FIGURE 6 Temperature and radial velocity calculated at $Ra = 5.0Ra_c$ and $E = 3 \times 10^{-4}$ for $\chi = 0.25$, 0.50, and 0.75. The same plotting conventions are used in Fig. 4.

Furthermore, some of the sheet-like flows bifurcate in radius such that the wavenumber increases at around mid-shell. Similar sheet-like, quasi-geostrophic, outwellings have been observed in supercritical rotating convection laboratory experiments by Sumita and Olson (2000) and have been inferred from experimental acoustic Doppler velocimetry measurements made by Aubert *et al.* (2001). Those experiments were both made in $\chi \sim 0.35$ devices and at Ekman numbers on the order of 5×10^{-6}. At those lower E values, they found higher wavenumber flows than we find in comparable numerical cases (e.g., Figure 4 in Sumita and Olson, 2000).

4 DISCUSSION

4.1 Effects of Imposed Symmetry

The Ra_c values determined for thick shells are dependent on the imposed longitudinal symmetry in the calculations. This dependence can be explained as follows. As Ra is increased, starting from subcritical values, steady state convection in the fluid is first achieved when $Ra = Ra_c$, characterized by m_c convection columns. In the full sphere calculations, all azimuthal wavenumbers up to $l_{\max}$ are allowed, which results in a more accurate prediction of Ra_c and m_c. In Table III, the critical azimuthal wave number is less than 4 in cases with $\chi \leq 0.25$. However, when 4-fold symmetry is imposed, the allowed azimuthal wavenumbers must be multiples of four. This requires Ra_c to increase to the value at which convection first occurs as an $m = 4$ instability. Similarly, the Ra_c value calculated using 8-fold symmetry for $\chi = 0.35$ represents the critical Rayleigh number for the onset of the $m = 8$ mode. At higher χ values, Ra_c is still affected by the imposed symmetry but less so as the percent difference between the full sphere m_c-value and the 4- and 8-fold symmetry m_c-values converge. The quasi-parabolic dashed curves in Fig. 2 also illustrate this behavior. These parabolic shapes demonstrate that a minimum Ra_c exists for solutions at each individual wavenumber.

4.2 Comparisons with Previous Work

4.2.1 Critical Rayleigh Number

In this section we compare our calculated values of the critical Rayleigh number (Ra_c), which are based on models with constant temperature at the inner and outer core boundaries, to the models of Jones *et al.* (2000) and Zhang (1992), which used internal heating.

Jones *et al.* (2000), calculated the critical Rayleigh number for the onset of convection in a rapidly rotating sphere (with no inner core) filled with a Boussinesq fluid and containing a uniform distribution of heat sources. Five different values of the Taylor number ($T = 4/E^2$) were used. The authors converted their Rayleigh number, referred to here as Ra_J, into a new Rayleigh number, referred to here as Ra_{JZ}, for comparison to Zhang's (1992) results for convection in a rapidly rotating spherical shell with a uniform distribution of heat sources. Equation 5.3 in Jones *et al.* (2000) is given by

$$Ra_{JZ} = (1 - \chi)^{10/3} Ra_J. \tag{12}$$

In Jones *et al.*'s (2000) study of flow in a full sphere, Ra_J depends only on the Taylor number T. Therefore, in the equation given above, Ra_{JZ} is a function of both χ and T.

Using the Ra_J values calculated at $Pr = 1$ in Jones *et al.* (2000), we calculate the corresponding Ra_{JZ} values using (12). These values are represented by the open circles in Fig. 7. Each dashed line in the figure corresponds to a different radius ratio (represented by a tag) and describes the asymptotic behavior of the critical Rayleigh number. With the slope of each dashed line equal to 2/3, we see that the critical Rayleigh number Ra_{JZ} is proportional to $T^{2/3}$ (or alternatively $E^{-4/3}$) for all the radius ratios shown.

To see how our results fit in Fig. 7, we must relate Ra to Ra_{JZ}. In our models Ra is defined in terms of the temperature difference, ΔT, between the inner and outer spherical shells. However, in Zhang's formulation, the Rayleigh number was defined in terms of the parameter β, related to the conductive temperature gradient ($\nabla T = -\beta \mathbf{r}$). For a given temperature difference between the inner and outer shells, it can be shown that

$$\beta = \frac{2\Delta T}{D^2}\frac{(1-\chi)}{(1+\chi)}. \tag{13}$$

By rewriting Ra_{JZ} in terms of ΔT and comparing the buoyancy term in the equations of motion, we arrive at the following relation

$$Ra_{JZ} = \frac{2(1-\chi)^2}{(1+\chi)}\,Ra. \tag{14}$$

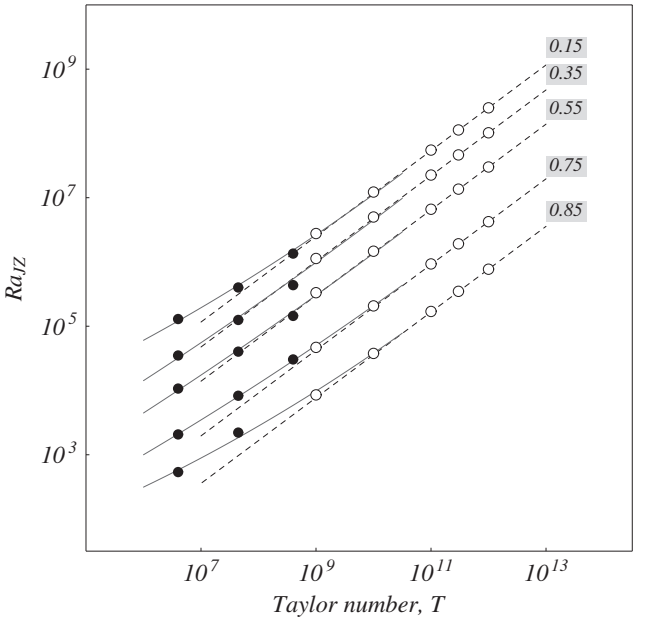

FIGURE 7 A log–log plot of Ra_{JZ} *vs* T. Open circles correspond to the critical Rayleigh numbers (Ra_J), defined and calculated by Jones *et al.* (2000), transformed using (12) to Ra_{JZ}. Solid circles correspond to the critical Rayleigh numbers (Ra_c), defined and calculated in this work, transformed using (14) to Ra_{JZ}. Each dashed line corresponds to a different radius ratio and describes the asymptotic behavior of the critical Rayleigh number. All dashed lines have slopes equal to 2/3.

The Ra_{JZ} values corresponding to our calculated critical Rayleigh numbers are represented by the solid circles in Fig. 7.

We can see that, in general, our values are a continuation of Jones *et al.*'s (2000) values extending to high Ekman number (i.e., low Taylor number) values. Our values do not lie exactly on the asymptotic dashed line, especially for the lowest and highest radius ratios. There are two explanations for such deviations. First, our results are not yet in the asymptotic regime. Second, the temperature profile of our model differs from that of Zhang's model. The temperature gradient in our models is proportional to $1/r^2$ causing the sharpest temperature drop to be close to the inner shell boundary. In Zhang's model, on the other hand, the temperature gradient is proportional to r causing the sharpest temperature gradient to be close to the outer shell boundary.

In Fig. 7, the average slope of the five continuous lines at $T = 1.1 \times 10^7$ is 0.58 ± 0.04. This average slope, which approximates $\gamma/2$, agrees well with our fit of $\gamma = 1.16$ in (10).

4.2.2 Critical Wave Number

The values of λ_c, obtained here as a function of the radius ratio χ, may be compared with approximations for the critical azimuthal wavelengths of convection columns in a rapidly rotating, uniformly heated sphere with no inner core. In the notation of Busse (1970), the values of λ_c at $Pr = 1$, which are presented in the third column of Table V show satisfactory agreement with our best fitting results. This implies that neither heating mode nor the radius ratio have significant effect on the critical azimuthal wavelength, λ_c, of the convection. However, the critical azimuthal wavenumber, m_c, is a strong function of the radius ratio χ. In the studies of Roberts (1968) and Busse (1970), they found convection to onset at a cylindrical radius of $s \simeq r_o/2$. We find that convection always onsets adjacent to the inner boundary. It follows that for $\chi \simeq 0.5$ (i.e., $r_i = r_o/2$), our spherical shell calculations produce convective planforms nearly identical to that of an internally heated sphere near Ra_c.

5 CONCLUSIONS

We have investigated the effects of varying spherical shell geometry over a broad range of radius ratios, χ, in a suite of three-dimensional rotating convection calculations. The calculations have been performed using co-rotating, isothermal, mechanically rigid boundaries at Prandtl number $Pr = 1$, over the radius ratio range $0.10 < \chi < 0.92$, for Rayleigh numbers $Ra < 5Ra_c$, and at the three Ekman numbers $E = 10^{-3}$, 3×10^{-4} and 10^{-4}. Our results show that the convection always onsets via columnar motions adjacent to the inner boundary equator. The azimuthal wavelength of columnar convection is found to be nearly independent of the style of thermal forcing and the shell geometry, such that the number of columns is proportional to r_i. We have derived a relation that describes the variation of the critical Rayleigh number over the entire range $0.1 \leq \chi \leq 0.92$ and at the three values of the Ekman number. The dependence of Ra_c on χ and on E was found to be broadly consistent with previous studies of rotating convection in spheres and spherical shells. Finally, our results provide a baseline for future studies of rotating convection and dynamo action where

the radius ratio is a critical parameter. Examples include studies comparing the convective dynamics of planets with different convective shell geometries and studies of planetary evolution with a growing inner core.

Acknowledgments

Support for Al-Shamali and Heimpel has been provided by NSERC. Support for Aurnou has been provided under NASA grants NAG5-4077 and NAG5-10165. We thank two anonymous referees for comments that greatly improved this article and Wicht for providing the dynamo code, MAGIC 2.0.

References

Aubert, J., Brito, D., Nataf, H.-C., Cardin, P. and Masson, J.-P., "A systematic experimental study of spherical shell convection in water and liquid gallium", *Phys. Earth. Planet. Inter.* **128**, 51–74 (2001).

Busse, F.H., "Thermal instabilities in rapidly rotating systems", *J. Fluid Mech.* **44**, 441–460 (1970).

Busse, F.H. and Carrigan, C.R., "Laboratory simulation of thermal convection in rotating planets and stars", *Science* **191**, 81–83 (1975).

Cardin, P. and Olson, P., "An experimental approach to thermochemical convection in the Earth's core", *Geophys. Res. Lett.* **19**, 1995–1998 (1992).

Cardin, P. and Olson, P., "Chaotic thermal convection ina rapidly rotating spherical shell: consequences for flow in the outer core", *Phys. Earth Planet. Inter.* **82**, 235–259 (1994).

Chandrasekhar, S., *Hydrodynamic and Hydromagnetic Stability*, New York, Oxford University Press (1961).

Christensen, U., Olson P. and Glatzmaier, G.A., "Numerical modeling of the geodynamo: a systematic parameter study", *Geophys. J. Int.* **138**, 393–409 (1999).

Dormy, E., "Modelisation Numerique de la Dynamo Terrestre", Ph.D. Thesis, Institut de Physique du Globe de Paris (1997).

Drew, S.J., "Thermal convection in a spherical shell with a variable radius ratio", *Geophys. Astrophys. Fluid. Dynam.* **59**, 165–183 (1991).

Glatzmaier, G.A. and Olson, P.L., "Highly supercritical thermal convection in a rotating spherical shell: centrifugal vs. radial gravity", *Geophys. Astrophys. Fluid. Dynam.* **70**, 113–136 (1993).

Jones, C.A., Soward, A.M. and Mussa, A.I., "The onset of thermal convection in a rapidly rotating sphere", *J. Fluid Mech.* **405**, 157–169 (2000).

Kono, M. and Roberts, P.H., "Definition of the Rayleigh number for geodynamo simulation", *Phys. Earth. Planet. Int.* **128**, 13–24 (2001).

Miesch, M.S., Elliott, J.R., Toomre, J., Clune, T.C., Glatzmaier, G.A. and Gilman, P.A., "Three-dimensional spherical simulations of solar convection: differential rotation and pattern evolution achieved with laminar and turbulent states", *Astrophys. J.* **532**, 593–615 (2000).

Morrison, G. and Fearn, D.R., "The influence of Rayleigh number, azimuthal wavenumber and inner core radius on 2-$\frac{1}{2}$ D hydromagnetic dynamos", *Phys. Earth. Planet. Inter.* **117**, 237–258 (2000).

Olson, P.L., and Glatzmaier, G.A., "Magnetoconvection in a rotating spherical shell: structure of flow in the outer core", *Phys. Earth. Planet. Inter.* **92**, 109–118 (1995).

Proudman, J., "On the motion of solids in a liquid possessing vorticity", *Proc. R. Soc. Lond.* A **92**, 408–424 (1916).

Roberts, P.H., "On the thermal instability of a rotating-fluid sphere containing heat sources", *Phil. Trans. Soc. Lond.* A **263**, 93–117 (1968).

Roberts, P.H. and Glatzmaier, G.A., "The geodynamo, past, present and future", *Geophys. Astrophys. Fluid Dynam.* **94**, 47–84 (2001).

Sakuraba, A. and Kono, M., "Effects of the inner core on the numerical solution of the magnetohydrodynamic dynamo", *Phys. Earth. Planet. Inter.* **111**, 105–121 (1999).

Schubert, G. and Zhang, K., "Effects of an electrically conducting inner core on planetary and stellar dynamos", *Astrophys. J.* **557**, 930–942 (2001).

Sumita, I. and Olson, P., "Laboratory experiments on high Rayleigh number thermal convection in a rapidly rotating hemispherical shell", *Phys. Earth. Planet. Inter.* **117**, 153–170 (2000).

Tilgner, A. and Busse, F.H., "Finite amplitude convection in rotating spherical fluid shells", *J. Fluid Mech.* **332**, 359–376 (1997).

Wicht, J., "Inner-core conductivity in numerical dynamo simulations", *Phys. Earth. Planet. Inter.* **132**, 281–302 (2002).

Yano, J.-I., "Asymptotic theory of thermal convection in rapidly rotating systems", *J. Fluid Mech.* **243**, 103–131 (1992).
Zhang, K. and Jones, C.A., "The influence of Ekman boundary layers on rotating convection", *Geophys. Astrophys. Fluid Dynam.* **71**, 145–162 (1993).
Zhang, K., "Spiraling columnar convection in rapidly rotating spherical shells", *J. Fluid Mech.* **236**, 535–556 (1992).
Zhang, K. and Greed, G.T., "Convection in a rotating annulus: An asymptotic theory and numerical solutions", *Phys. Fluids* **10**, 2396–2404 (1998).